Supporting Information

Siderophore-Inspired Two-Dimensional Fe-Hydroxamate Metal-Organic Framework

*Wenlei Tang,[a] Zhen-Wu Shao,[a] Li Xiong,[a] Zhiyuan Zhang,[a] Kaiyuan Tan,[a] Xuan Feng,[a] Wenjing Wu,[a] and Chong Liu[a]**

[a] School of Chemical Engineering, Sichuan University, Chengdu 610065, China

Email: liuchong@scu.edu.cn (C.L.)

Contents

1. General information

All purchased chemicals were used without further purification except where otherwise noted.

Single-crystal X-ray diffraction (SC-XRD) data for SUM-31 on a Bruker D8 Venture Metaljet Photon III diffractometer. The crystal was kept at 193.00 K during data collection. Using Olex2,[1] the structure was solved with the SHELXT[2] structure solution program using Intrinsic Phasing and refined with the SHELXL[3] refinement package using Least Squares minimization.

Powder X-ray diffraction (PXRD) patterns were collected using a Rigaku MiniFlex600 operating at 40 kV, 40 mA for Cu Kα, (λ = 1.54178 Å) with a scan speed of 10° min^{-1} from 3 to 50° at a step size of 0.01°.

^{1}H NMR spectrum was collected on a JNM-ECZ400S/L1 (400 MHz) spectrometer (JEOL Ltd., Tokyo, Japan).

Thermogravimetric analysis (TGA) was carried out on a TA Discovery SDT 650 simultaneous thermal analyzer from room temperature to 800 °C at a heating rate of 10 °C min^{-1} in a N_2 flow of 100 mL min^{-1}.

N_2 adsorption-desorption experiments were performed on a BELSORP MAX instrument at 77 K. Activation procedure is described in Section 3.3.

CHNS elemental Analysis was carried out on an Elemantar Vario UniCube instrument.

Electrochemical experiments were conducted on a CHI 660E electrochemical workstation (Shanghai CH Instruments Inc., China) in a three-electrode system, details are given in section 4.

Optical images were acquired with a Rui Hong BM-500T optical microscope.

Table S1. Structural information of different hydroxamate-containing MOFs

MOF	Metal	Linker	M–O(hydroxyl) (Å)	M–O(carbonyl) (Å)	Ref.
SUM-1(Zr)	Zr	H_2-BDHA	2.158	2.214	4
SUM-1(Hf)	Hf	H_2-BDHA	2.158	2.167	4
SUM-9	In	H-BDHA	2.132/2.118/2.158	2.165/2.176/2.164	5
MUV-11	Ti	H_2-BDHA	2.109/2.08/2.108	2.127/2.136/2.154	6
Fe-HAF-1	Fe	H_4-BPTH	1.977	2.03	7
Fe-HAF-2	Fe	H_4-TPTH	2.016/2.018/2.018	2.082/2.082/2.083	8
Tl-MOF	Tl	H_2-MHA	2.593/2.885	2.723/2.739	9

2. Synthesis of ligand and MOF

2.1 Synthesis of *E*-H_2edh

The synthesis of ligand *E*-ethylenedihydroxamic acid (*E*-H_2edh) was carried out according to the procedure previously reported[10]. The identity and purity of the ligand were confirmed by ^{1}H NMR (Figure S1).

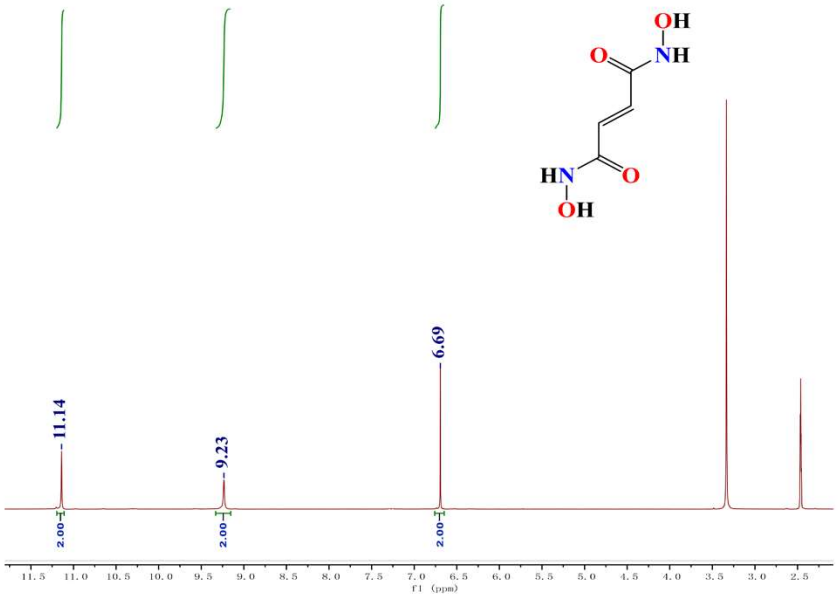

Figure S1. ^{1}H NMR spectrum of *E*-H_2edh in DMSO-d_6.

2.2 Synthesis of SUM-31

E-H_2edh (27.0 mg, 0.185 mmol) and $Fe(NO_3)_3 \cdot 9H_2O$ (12.0 mg, 0.0297 mmol) were mixed with DMF (0.750 mL) and DMSO (0.250 mL) in a 4-mL glass vial before tightly capped and briefly sonicated. The mixture was heated in an isothermal oven at 100 ℃ for 24 hours. After cooling to room temperature, maroon block-shaped crystals (Figure S2) were collected and washed with DMF.

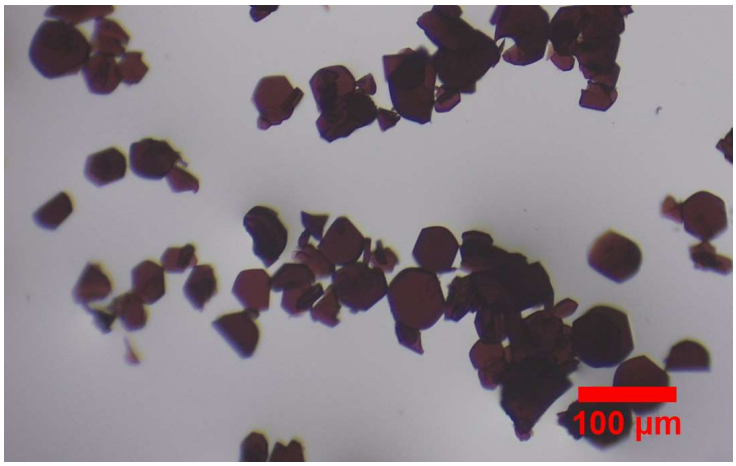

Figure S2. Optical image of large SUM-31 crystals.

Additionally, SUM-31 could also be prepared in smaller sizes for electrochemical experiments, simply by decreasing the temperature and concentration. *E*-H_2edh (9.7 mg, 0.0665 mmol) and $Fe(NO_3)_3 \cdot 9H_2O$ (6.0 mg, 0.0149 mmol) were mixed with DMF (0.92 mL) and DMSO(0.08 mL) in a 4-mL glass vial before tightly capped and briefly sonicated. The mixture was heated in an isothermal oven at 80 °C for 24 hours. After cooling to room temperature, the crystals (Figure S3) were collected and washed with DMF.

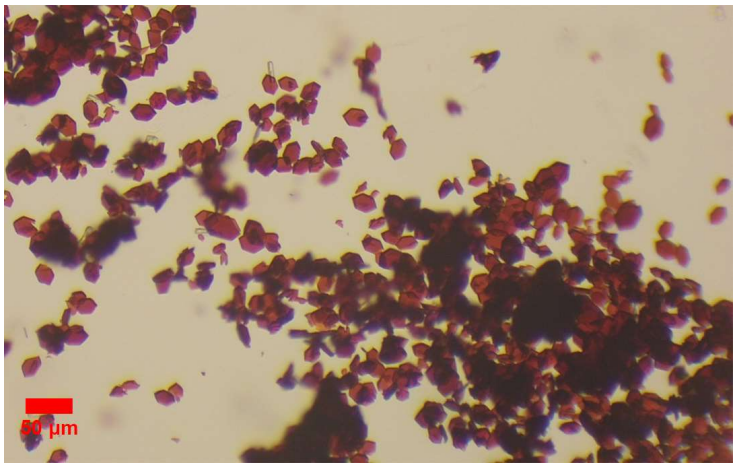

Figure S3. Optical image of small SUM-31 crystals.

3. Characterization of MOFs

3.1 Crystallographic study of SUM-31

Table S2. Crystal data and structure refinement details for SUM-31

CCDC depository number	2223527
Identification code	SUM-31
Empirical formula	$C_{12}H_{12}Fe_2N_6O_{12}$
Formula weight	543.98
Temperature/K	193.00
Crystal system	monoclinic
Space group	C2/c
a/Å	13.635(18)
b/Å	21.87(2)
c/Å	17.252(18)
α = γ/°	90
β/°	111.89(5)
Volume/Å^3	4773(10)
Z	4
ρ_{calc}g/cm^3	0.757
μ/mm^{-1}	3.568
F(000)	1096.0
Crystal size/mm^3	0.12 × 0.1 × 0.1
Radiation	GaKα (λ = 1.34139)
2Θ range for data collection/°	7.022 to 121.594
Index ranges	-17 ≤ h ≤ 17, -27 ≤ k ≤ 26, -22 ≤ l ≤ 16
Reflections collected	15851
Independent reflections	5217 [Rint = 0.0877, Rsigma = 0.1073]
Data/restraints/parameters	5217/139/191
Goodness-of-fit on F2	0.965
Final R indexes [I>=2σ (I)]	R1 = 0.0922, wR2 = 0.2820
Final R indexes [all data]	R1 = 0.1491, wR2 = 0.3227
Largest diff. peak/hole / e Å^{-3}	0.54/-0.71

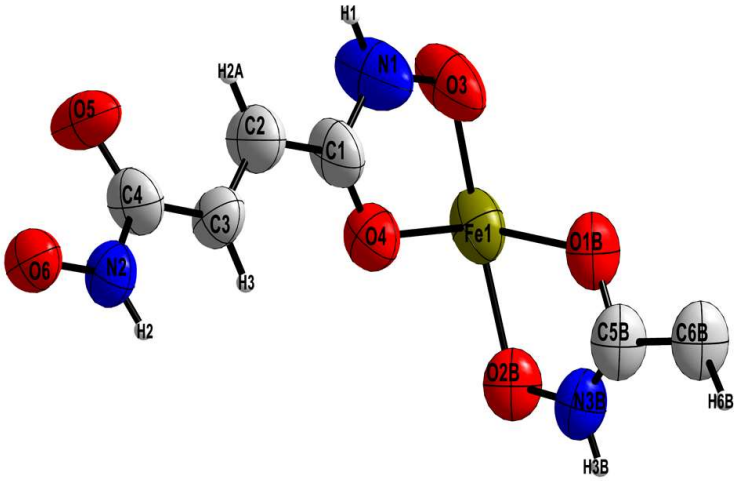

Figure S4. ORTEP diagram of the asymmetric unit of SUM-31 (50% probability factor for the thermal ellipsoids), with disorders removed, generated in Diamond 3.2k.

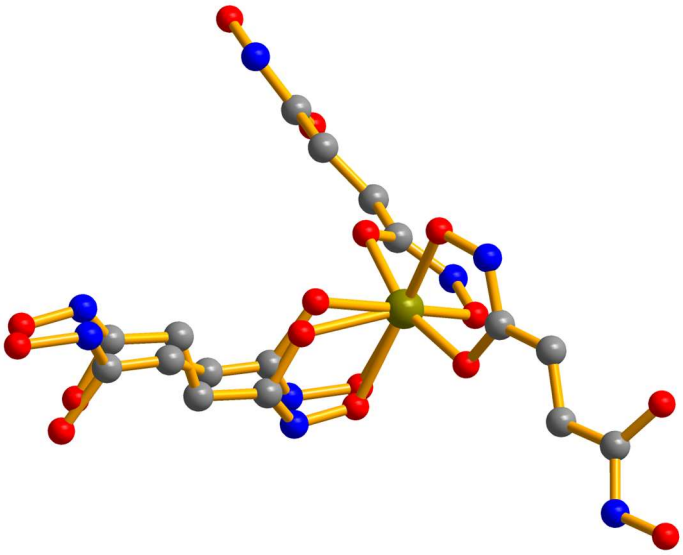

Figure S5. Coordination environment of the homoleptic Fe(*E*-edh)$_3$ moiety in SUM-31, showing disorder as determined by SC-XRD.

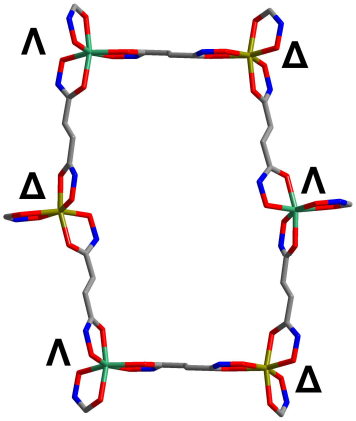

Figure S6. Racemic Fe(hydroxamate)$_3$ centers of Δ and Λ configurations in a hexagonal ring of SUM-31.

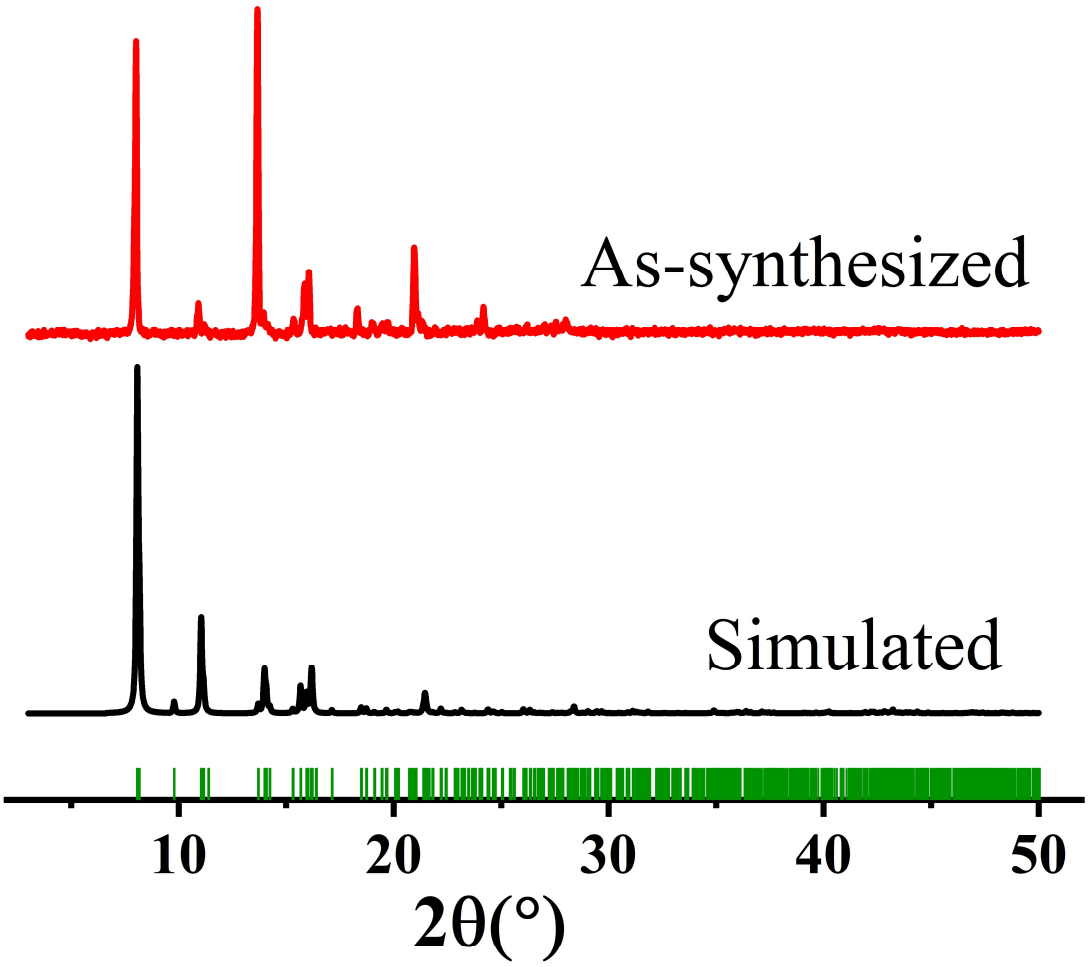

Figure S7. PXRD patterns comparing the simulated (black) and experimental (red), with calculated peak positions indicated by green bars.

Table S3. Fe–O bond lengths of CSD-mined structures and SUM-31

Refcode	Fe–O(carbonyl)$_{min}$ (Å)	Refcode	Fe–O(hydroxyl)$_{min}$ (Å)
This work	**1.923**	SEMKOM	1.913
DEWNAU	1.971	FEROXE10	1.938
DEWNAU	1.974	**This work**	**1.938**
WAKXAH	1.974	SUXREI	1.946
XUPVIP	1.974	UDAWUS	1.948
DORGEX	1.978	FTAFUS10	1.949
COFDIK10	1.986	DUPJON	1.95
JEPRAX	1.995	TEQKUV	1.952
QERKUW	1.995	TEQKUV01	1.952
UDAXAZ	1.997	BURDIB	1.953
COFDIK10	2.008	FERCRN10	1.955
BOPMUO01	2.009	EKOTUV	1.96
UDAWUS	2.009	OCELOX	1.961
EKOTOP	2.010	UNEVUE	1.961
OCELOX	2.011	CUJHIY	1.962
YOLBUX	2.012	JEPRAX	1.962
UNEVUE	2.014	QUXXOX	1.962
CUJHIY	2.016	CETWIH	1.963
EKOTAB	2.016	COFDIK10	1.963
CUJHOE	2.019	EKOVAD	1.963
EKOTIJ	2.020	IRADEK	1.964
EKOTUV	2.020	QOZDUE	1.964
FERMAH11	2.020	TEQKUV	1.964
UDAWUS	2.020	TEQKUV01	1.964
IRADEK	2.021	SISSAO	1.966
EKOVAD	2.022	BUHQUQ	1.967
FERCRN10	2.023	FERCRN10	1.967
YOLBUX	2.023	FERMAH11	1.967
FERRID10	2.024	FERRID10	1.967
UNEWEP	2.024	IRADEK	1.967
SUXREI	2.026	OGULUA	1.968
QERKUW	2.028	SIPMEJ	1.968
QOZDUE	2.028	FEBOAH01	1.969
CUJHIY	2.029	COFDIK10	1.971
OFUYET	2.029	OFUYET	1.971
UNEWAL	2.029	OGULUA	1.971
SEMKOM	2.031	OGULUA	1.971
FTAFUS10	2.032	SUXREI	1.973
TEQKUV	2.032	BOPMUO01	1.974
TEQKUV01	2.032	FEBOAH	1.974

FERCRN10	2.033	FEBOAH02	1.975
TEQKUV	2.033	SISSES	1.975
TEQKUV01	2.033	UNEWEP	1.975
OGULUA	2.035	IRADEK	1.977
BUHQUQ	2.036	QERKUW	1.977
FEBOAH01	2.036	UDAXAZ	1.977
SISSAO	2.036	CUJHOE	1.979
SUXREI	2.036	EKOTIJ	1.981
FEBOAH	2.039	OGUMAH	1.981
IRADEK	2.039	VAYYEB	1.981
OGULUA	2.041	CUJHIY	1.982
SIPMEJ	2.042	IRADEK	1.983
DUPJON	2.044	UDAWUS	1.984
OGULUA	2.044	YOLBUX	1.984
QUXXOX	2.044	YOLBUX	1.985
SISSES	2.044	EKOTAB	1.986
OGUMAH	2.047	UNEWAL	1.986
VAYYEB	2.048	OGULUA	1.991
FEBOAH02	2.049	DEWNAU	1.993
FEROXE10	2.050	EKOTOP	1.996
OGULUA	2.054	QERKUW	1.997
BURDIB	2.055	DORGEX	2.002
IRADEK	2.058	DEWNAU	2.004
CETWIH	2.059	WAKXAH	2.013
IRADEK	2.066	FAVFER	2.016
FAVFER	2.082	XUPVIP	2.017

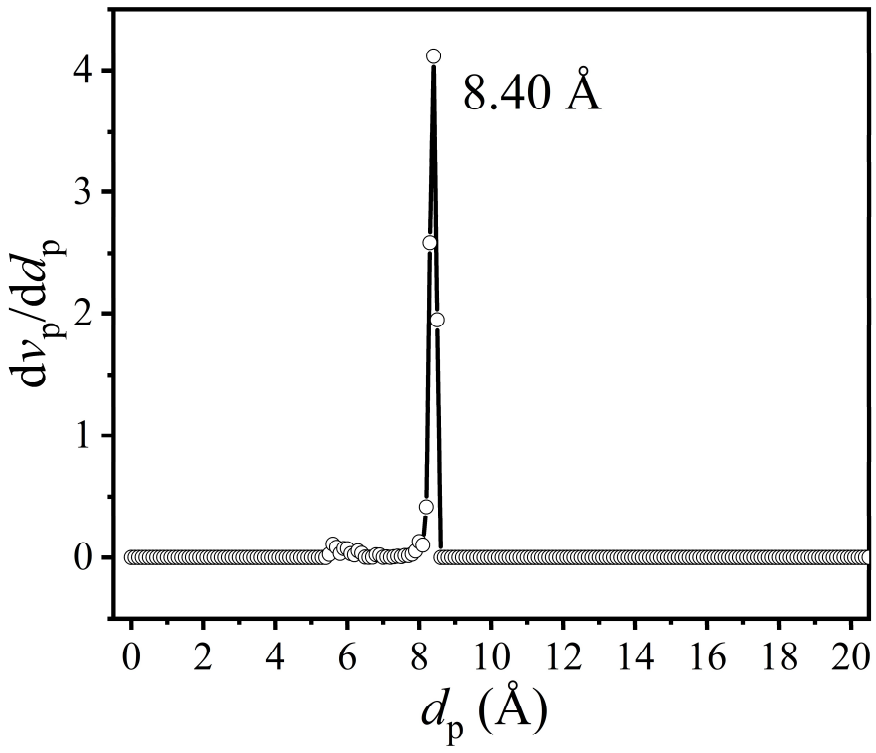

Figure S8. Pore size distribution plot of SUM-31 as calculated by Zeo++.[11]

3.2 Composition analysis of SUM-31

For TGA and CHNS elemental analysis, the as-synthesized MOF crystals were washed with dry DMF (3X), ethanol (3X) and dried with N_2 flow until they became free-flowing solids.

For TGA, the solid sample was loaded into a ceramic pan for analysis (Fig. 2b in the main text). The ca. 31.12% weight loss corresponds to a composition of $Fe_8(edh)_{12}\cdot 3DMSO\cdot 13.5DMF$.

For CHNS elemental analysis, C: calc. 33.39%, found 32.82%; H: calc. 4.72%, found 5.35%; N: calc. 15.46%, found 15.39%; S: calc. 2.83%, found 3.00%.

Of note, SC-XRD data (solvent mask) revealed a presence of 796.5 (solvent) electrons per unit cell, which corresponds to a solvent content of

ca. 3DMSO·16.5DMF. The discrepancy was reasonable considering that the crystal was fully solvated when mounted for SC-XRD analysis comparing to a N_2-dried sample for TGA/CHNS elemental analysis.

3.3 N_2 sorption of SUM-31

As-synthesized SUM-31 MOFs crystals of smaller sizes (section 2.2) were washed with dry DMF (3X) and exchanged with ethanol (3X) for 72 hours. Then the crystals were activated using a Tousimis Samdri PVT-3D critical dryer before transferred to the degassing station of BELSORP MAX for 12 hours of degassing at room temperature. N_2 adsorption-desorption isotherms (Figure S9) were acquired at 77 K, and the Brunauer-Emmett-Teller (BET) surface area of SUM-31 was calculated to be only 29.88 $m^2 g^{-1}$. After sorption, the MOF crystals were examined using PXRD (Figure S10) and then loaded into a ceramic pan for TGA (Figure S11).

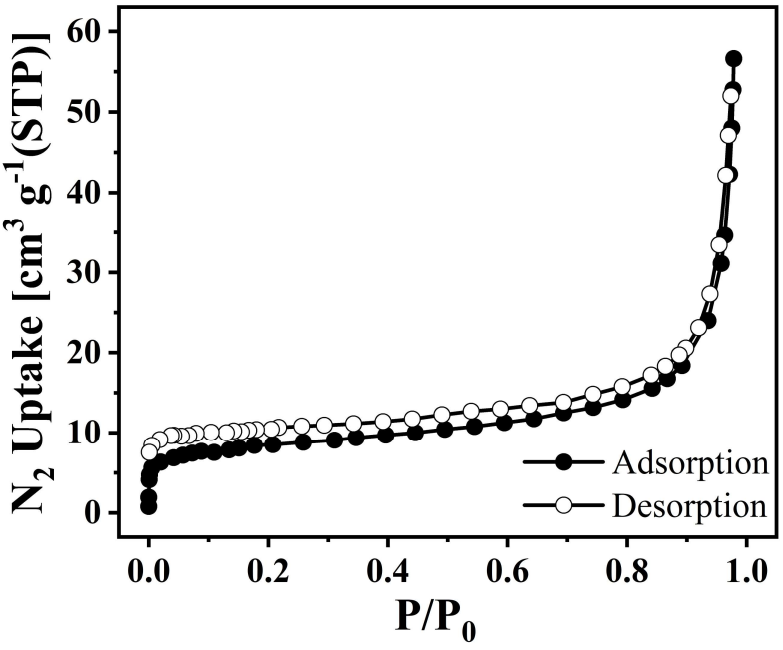

Figure S9. N_2 adsorption-desorption isotherms of SUM-31 at 77 K.

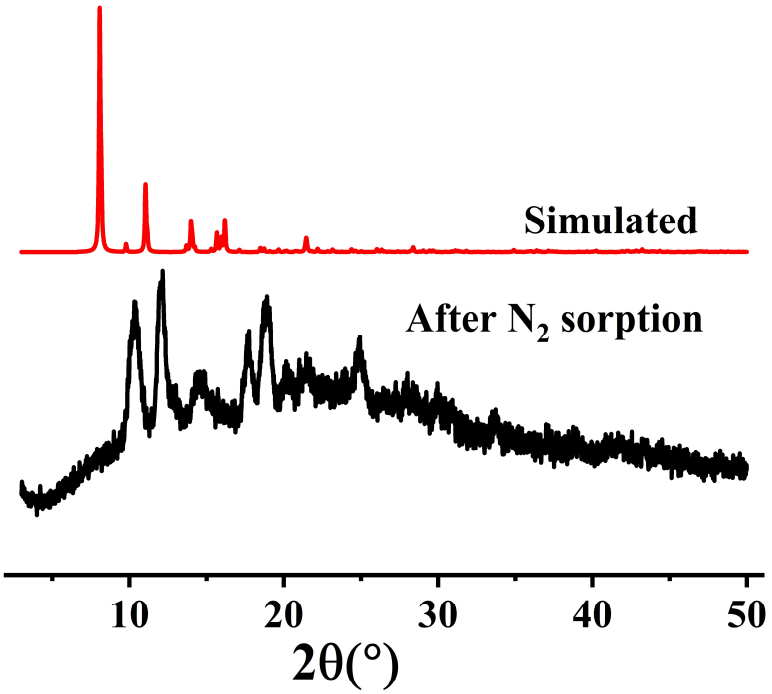

Figure S10. PXRD patterns of SUM-31 comparing the simulated (red) and experimental after N_2 sorption (black).

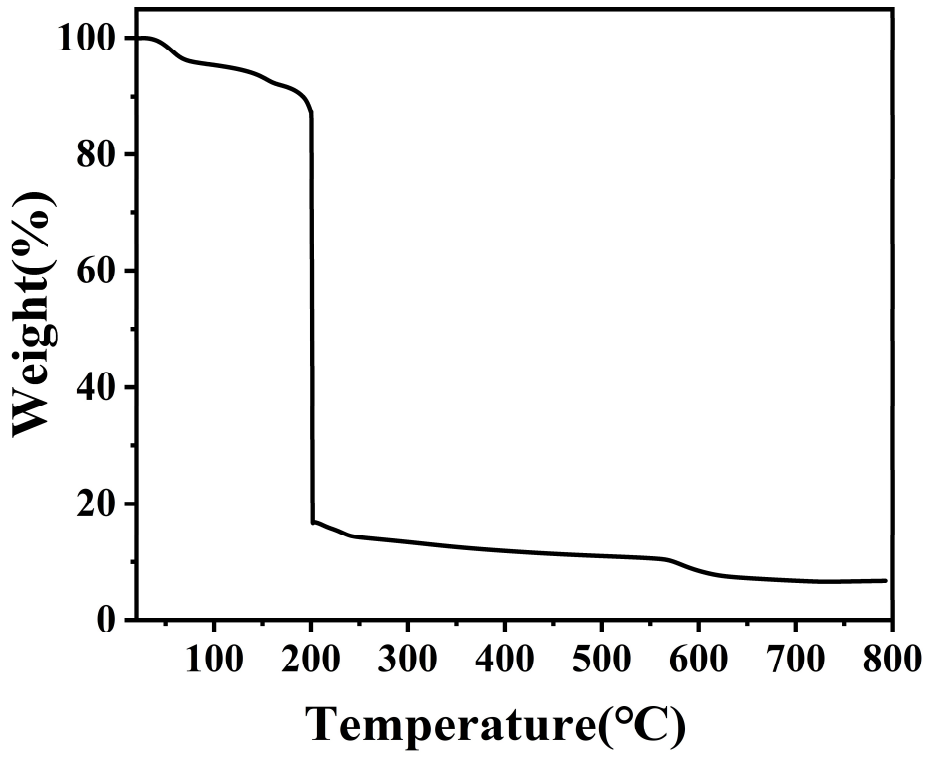

Figure S11. TGA plot of SUM-31 after N_2 sorption.

3.4 Stability of SUM-31

For aqueous solution treatments, the as-synthesized MOF crystals were washed with dry DMF(3X) and aqueous solutions of various pH values (2X) before soaked in the respective pH solution for 24 hours. Then the crystals were examined with PXRD.

4. Electrochemical experiments

Electrochemical experiments were conducted with a CHI 660E electrochemical workstation (Shanghai CHI Instrument Co., China) in a three-electrode system. The modified glassy carbon electrode (GCE), a saturated calomel electrode (SCE), and a Pt foil (1 cm^2) were used as the working electrode, reference electrode, and counter electrode, respectively.

For the electrolyte solutions in electrochemical experiments, an aqueous solution of pH = 10.25 was prepared by adding KOH to 0.1 M K_2HPO_4. Aqueous solutions of pH = 4.53 and pH = 6.98 were prepared by adjusting the ratios of 0.1 M K_2HPO_4 and 0.1 M NaH_2PO_4. Before each experiment, the electrolyte solution was purged with N_2 for 15 min to remove residual dissolved oxygen.

Cyclic voltammetry (CV) of the working electrode was tested at a scan rate of 100 mV s^{-1}. Differential pulse voltammogram (DPV) was acquired with the pulse amplitude, pulse width, and pulse period set to be 50 mV s^{-1}, 50 ms, and 500 ms, respectively.

4.1 Preparation of SUM-31 aqueous suspension

The as-synthesized SUM-31 crystals of smaller sizes (section 2.2) were centrifuged and washed with DMF (2X) and ethanol (2X) before drying in vacuo. 1.5 mg of SUM-31 samples were mixed with 1 mL of ethanol and grinded for 10 min to obtain a uniform aqueous suspension.

4.2 Preparation of SUM-31/GCE working electrode

GCE was polished successively with 1.0 mm, 0.3 mm, and 0.05 mm alumina slurry on a polishing cloth (Buehler, Esslingen, Germany) to produce a mirror-like surface. Then, it was sonicated with ethanol/water (1:1, v/v) solution for 10 min and dried by N_2 gas stream. Next, 10 μL of the abovementioned SUM-31 aqueous suspension (1.5 mg mL^{-1}) was coated onto the GCE bare surface and dried at room temperature. 10 μL of a 0.05% Nafion solution, which was obtained by diluting 5% Nafion ethanol/water (1:1 v/v) solution with ethanol, was dropped onto the surface of the composites and dried at 50 °C for 1 h.

4.3 CV and DPV analysis

The proposed electrochemical mechanism is shown below:

$$SUM-31-Fe^{II} - e^{-} \rightarrow SUM-31-Fe^{III} \quad (1)$$

$$2SUM-31-Fe^{III} + 2OH^{-} + H_2O_2 \rightarrow 2SUM-31-Fe^{II} + 2H_2O + O_2 \quad (2)$$

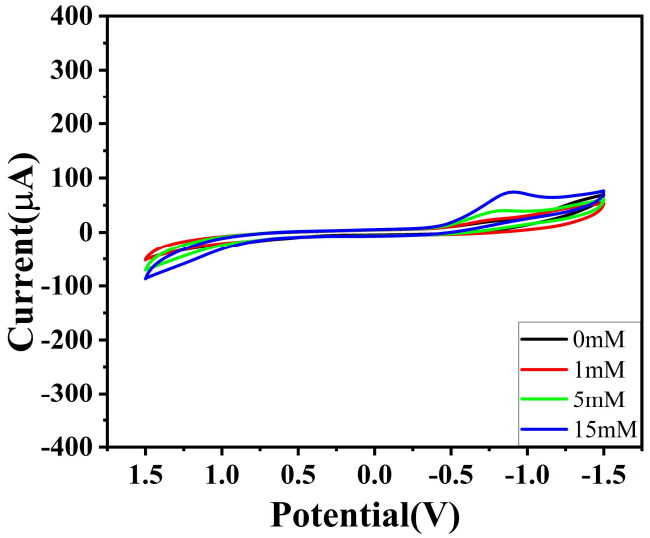

Figure S12. CV curves of SUM-31/GCE electrode at a scan rate of 100 mV/s in electrolyte (pH = 4.53) containing 0 to 15 mM H_2O_2.

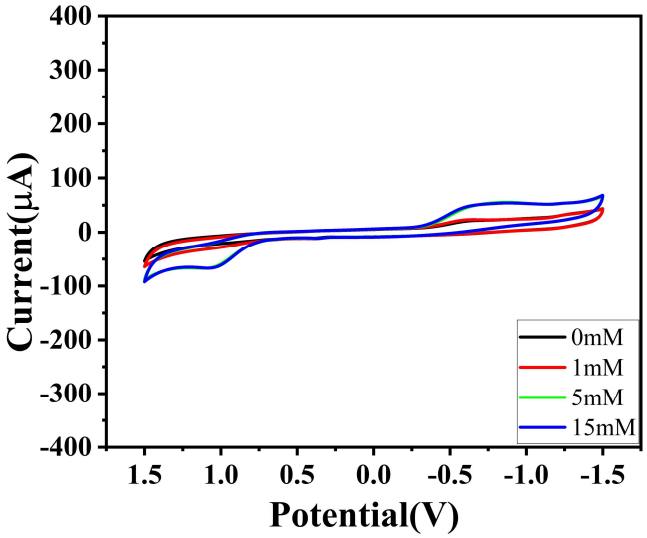

Figure S13. CV curves of SUM-31/GCE electrode at a scan rate of 100 mV/s in electrolyte (pH = 6.98) containing 0 to 15 mM H_2O_2.

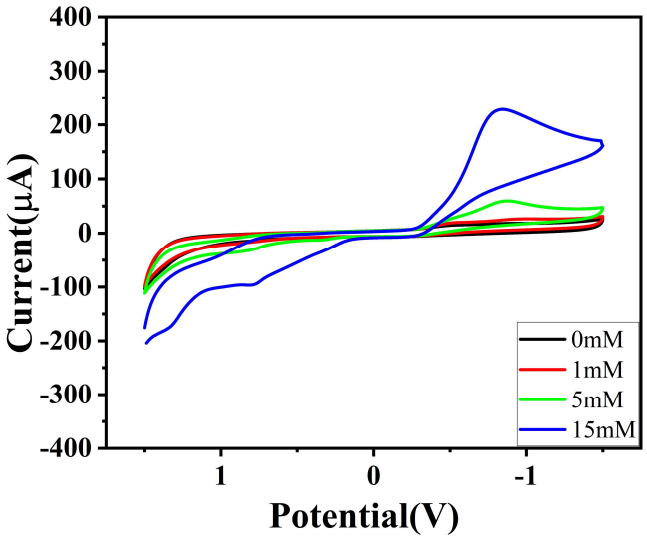

Figure S14. CV curves of SUM-31/GCE electrode at a scan rate of 100 mV/s in electrolyte (pH = 10.25) containing 0 to 15 mM H_2O_2.

For the blank control experiment without SUM-31, 0.05% Nafion

solution was dropped onto the surface of the GCE (pre-treated as described in section 4.2) and dried at 50 °C for 1 h.

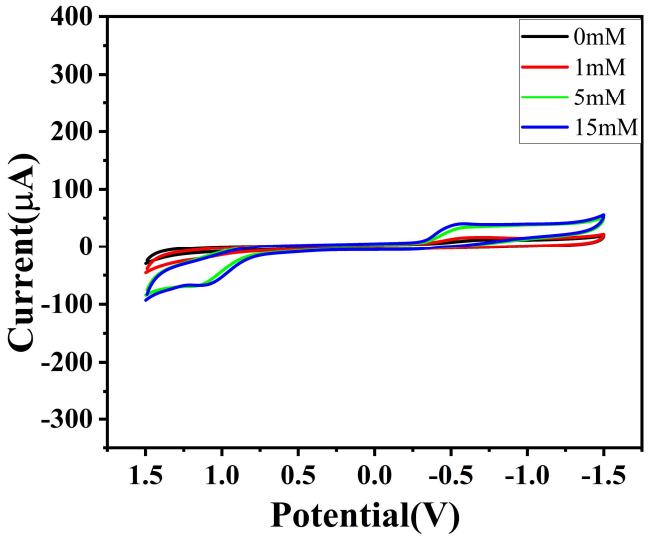

Figure S15. CV curves of GCE electrode at a scan rate of 100 mV/s in electrolyte (pH = 10.25) containing 0 to 15 mM H_2O_2.

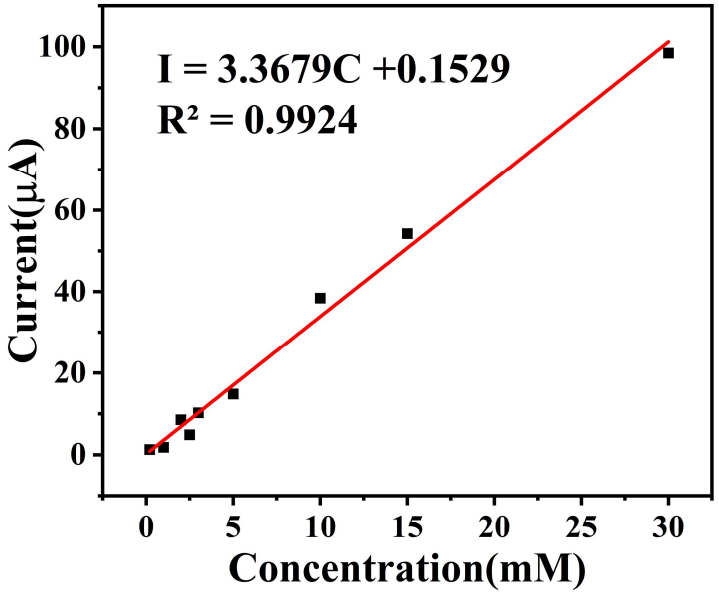

Figure S16. Enlarged Fig. 3b inset of the main text: the linear relationship between the currents and the concentrations of H_2O_2.

Table S4. Comparison of select reported H_2O_2 sensors

Electrode material	Method	Linear range (mM)	Detection limit (μM)	Ref.
Ag NW array	i-t	0.1–3.1	29.2	12
Co-MOF	i-t	n/a	2.9	13
CuMOFs@FeP-pSC4-AuNPs	DPV	0.5–2.5	47	14
CNP-CuMOF	CV	1–20	n/a	15
rGO-Au	i-t	1.5–7.6	19	16
ITO/(PEDOT-PdBI-*co*-HKCN)/GOx	i-t	0.25–2.5	176	17
MnO_2 nanowires/ERGO paper	i-t	0.1–45.4	10	18
PCS/HB/CPE	CV	0.1–5	32	19
SUM-31	DPV	0.2–30	1.4	This work

5. References

1. O. V. Dolomanov, L. J. Bourhis, R. J. Gildea, J. A. K. Howard and H. Puschmann, *J. Appl. Cryst.,* **2009**, *42*, 339-341.

2. G. M. Sheldrick, *Acta. Crystallogr. A*, **2015**, *71*, 3-8.

3. G. M. Sheldrick, *Acta. Crystallogr. C*, **2015**, *71*, 3-8.

4. Q. Lai, Z. Q. Chu, X. Xiao, D. Dai, T. Song, T. Y. Luo, W. Tang, X. Feng, Z. Zhang, T. Li, H. Xiao, J. Su and C. Liu, *Chem. Commun.*, **2022**, *58*, 3601-3604.

5. X. Feng, Z. Qin, Q. Lai, Z. Zhang, Z.-W. Shao, W. Tang, W. Wu, Z. Dai and C. Liu, *Sep. Purif. Technol.*, **2023**, *305*, 122476.

6. N. M. Padial, J. Castells-Gil, N. Almora-Barrios, M. Romero-Angel, I. da Silva, M. Barawi, A. Garcia-Sanchez, V. A. dela Pena O'Shea and C. Marti-Gastaldo, *J. Am. Chem. Soc.*, **2019**, *141*, 13124-13133.

7. J. A. Chiong, J. Zhu, J. B. Bailey, M. Kalaj, R. H. Subramanian, W. Xu, S. M. Cohen and F. A. Tezcan, *J. Am. Chem. Soc.*, **2020**, *142*, 6907-6912.

8. J. Zhu, L. Samperisi, M. Kalaj, J. A. Chiong, J. B. Bailey, Z. Zhang, C. J. Yu, R. E. Sikma, X. Zou, S. M. Cohen, Z. Huang and F. A. Tezcan, *Dalton. T.*, **2022**, *51*, 1927-1935.

9. S.-H. Huang, R.-J. Wang and T. C. W. Mak, *J. Chem. S., Dalton Trans.*, **1991**, *5*, 1379-1381.

10. J. B. Bailey, L. Zhang, J. A. Chiong, S. Ahn and F. A. Tezcan, *J. Am. Chem. Soc.*, **2017**, *139*, 8160-8166.

11. T. F. Willems, C. H. Rycroft, M. Kazi, J. C. Meza, M. Haranczyk, *Micropor. Mesopor. Mater.*, **2012**, *149*, 134-141

12. E. Kurowska, A. Brzózka, M. Jarosz, G. D. Sulka and M. Jaskuła, *Electrochim. Acta.*, **2013**, *104*, 439-447.

13. M. Zhang, G. Wang, B. Zheng, L. Li, B. Lv, H. Cao and M. Chen, *Nanoscale* **2019**, *11*, 5058-5063.

14. X. Hu, Y. Huang, J. Chen, X. Zhu, Z. Mao, Y. Wang, R. Hu and H. Chen, *Sensor. Actuat. B-Chem.*, **2021**, *342*, 130076.

15. M. Hesari, R. Jia and M. V. Mirkin, *Chem. Electro. Chem.*, **2022**, *9*, e2022003.

16. X. Liu, T. Shen, Z. Zhao, Y. Qin, P. Zhang, H. Luo and Z.-X. Guo, *Mater. Lett.*, **2018**, *229*, 368-371.

17. T. Y. Tekbasoglu, T. Soganci, M. Ak, A. Koca and M. K. Sener, *Biosens. Bioelectron.*, **2017**, *87*, 81-88.

18. Y. Shim, M. H. Nam, S. W. Hyuk, S. Y. Yoon and J. M. Song, *Anal. Chim. Acta.*, **2015**, *853*, 501-507.

19. V. Gautam, K. P. Singh and V. L. Yadav, *Int. J. Biol. Macromol.*, **2018**, *111*, 1124-1132.